Plume Measurements and Miniaturization of the Hall Thrusters with Circular Cross-sectional Discharge Chambers

IEPC-2005-051

Presented at the 29th International Electric Propulsion Conference, Princeton University, October 31 – November 4, 2005

Atsushi Shirasaki*, and Hirokazu Tahara†

Department of Mechanical Science and Bioengineering

Graduate School of Engineering Science, Osaka University

1-3, Machikaneyama, Toyonaka, Osaka 560-8531, JAPAN

Abstract: Plume measurements of Hall thruster with circular cross-sectional discharge chamber, named TCHT-2 were carried out. Ion current density measurement showed that the plume divergent angle was not sensitive to propellant mass flow rate and that the propellant utilization decreased as the mass flow rate decreased. Ion energy measurement using RPA indicated that the efficiency of acceleration decreases at low mass flow rate. From the electron temperature and plasma potential distribution inside the discharge chamber obtained by a double probe, the ionization/acceleration region is located at which strong radial magnetic field exists. The miniature Hall thruster TCHT-3A showed that thrust performance declines with scaling down by increase of ion loss. By applying strong radial magnetic field at the downstream region, miniature Hall thruster TCHT-3B achieved higher thrust performance than TCHT-3A did at low power level. It has efficiency (26-39%) in the power range 80-170W.

I. Introduction

The application of small satellites is useful for reducing the costs and risk of various missions. These satellites require small, low power and high performance propulsion devices. The Hall thruster is a promising propulsion device in space because of its high efficiency and thrust density. However, reducing Hall thruster dimension and input power results in significant decline of thrust performance[1-3].

According to simple scaling law of Hall thruster design[4], magnetic flux density applied in a Hall thruster is inversely proportional to thruster dimension. This results in magnetic saturation of the magnetic circuit, especially inner pole piece. Accordingly, it is difficult to apply appropriate magnetic field. Furthermore, volume-to-surface ratio (the ratio of volume of discharge chamber to its surface area) decreases as the thruster dimension decreases, and ion loss to the wall increases. That means simple downsizing conventional Hall thruster leads to not only low performance but also critical overheating and erosion of the thruster parts. Hence, special design is required for low power Hall thruster.

* Graduate Student, sirasaki@arl.me.es.osaka-u.ac.jp

† Associate Professor, tahara@me.es.osaka-u.ac.jp

Raitses et al. proposed a cylindrical Hall thruster that has circular cross-sectional ceramic discharge chamber[5]. Because of larger volume-to-surface ratio of the thruster, it suppresses increase in ion loss accompanied by downsizing Hall thruster. Smirnov et al. designed and investigated miniature cylindrical Hall thruster, and their thruster achieved thrust efficiency of 15-32% in the power range of 50-300W[6-8]. However, their cylindrical Hall thrusters have also coaxial part in the discharge chamber like conventional SPT. This coaxial part can cause the same problems as SPT. Hence, we eliminated coaxial part from the Hall thruster, named TCHT-2, with a circular cross-sectional discharge chamber[9]. Stable operation was achieved by means of TCHT-2 without coaxial part. Furthermore, TCHT-2 without coaxial part achieved higher thrust performance than TCHT-2 with coaxial part. In this study, we carried out plume measurements using TCHT-2 without coaxial part to understand performance characteristics and to find the ionization/acceleration region which are necessary to miniature Hall thrusters with circular cross-sectional discharge chambers. Then, we designed miniature Hall thruster and examined the thrust performance.

II. Experimental Setup

A. Thruster and vacuum facility

Figure 1 shows the cross-sectional view of TCHT-2 for plume measurement, which has a circular cross-sectional discharge chamber. The discharge chamber consists of only a circular cross-sectional part with no coaxial part. The anode located at the upstream end of the circular cross-sectional part is made of copper. The length of the discharge chamber is 25 mm. The radius of the discharge chamber is 28mm. The thruster has magnetic coils on the central axis and on the inner surface of the outer cylinder. Figure 2 shows the cross-sectional view of TCHT-3. The length and radius of the discharge chamber are 16mm and 14mm, respectively. TCHT-3 were classified into TCHT-3A and TCHT-3B. TCHT-3A has outer coil and center permanent magnet, and iron was used as the part indicated by the symbol (＊). In the case of TCHT-3B, a ring-like permanent magnet was used as the part instead of iron. The ring-like permanent magnet consists of six segmented magnet, and the magnetization

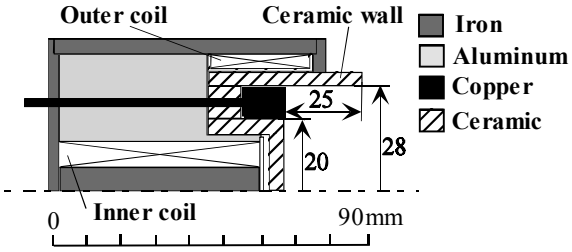

Figure 1. Cross-sectional view of TCHT-2

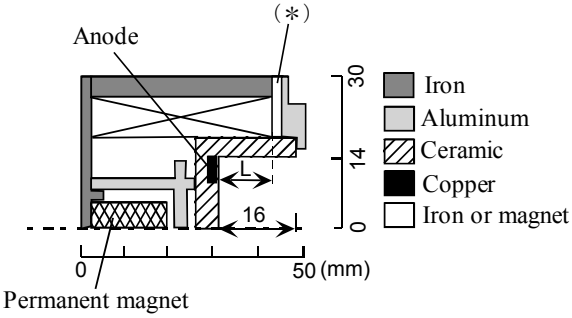

Figure 2. Cross-sectional view of TCHT-3

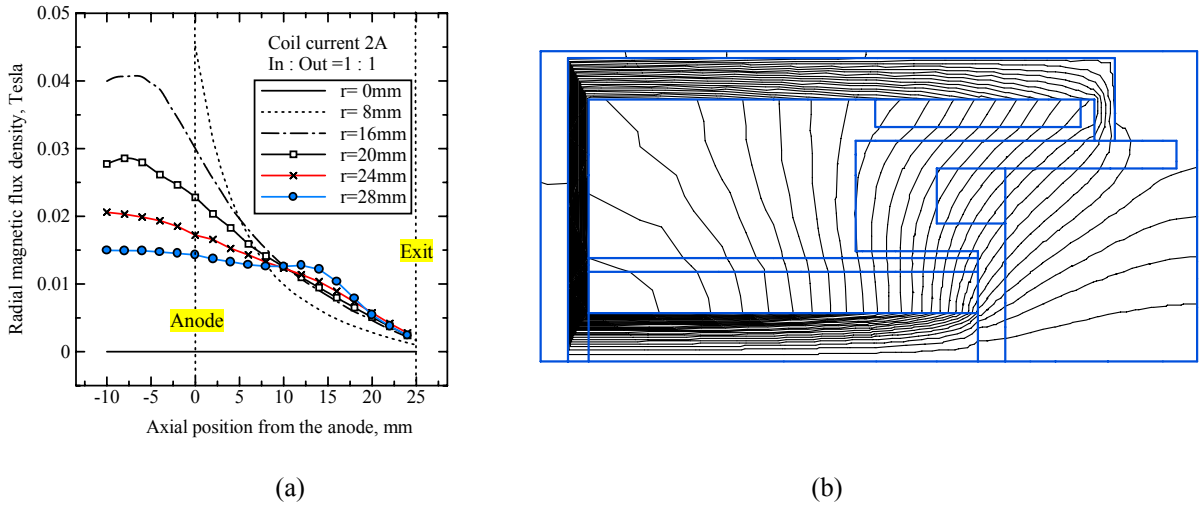

Figure 3. Magnetic field profiles of TCHT-2, (a)Axial profiles of radial magnetic flux density, (b)Magnetic field lines.

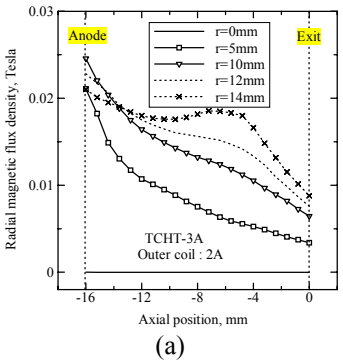

(a)

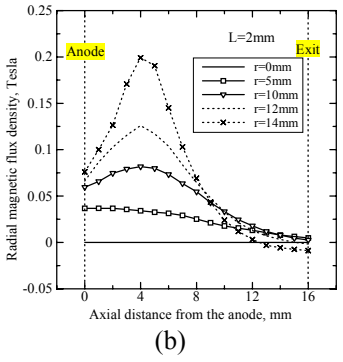

(b)

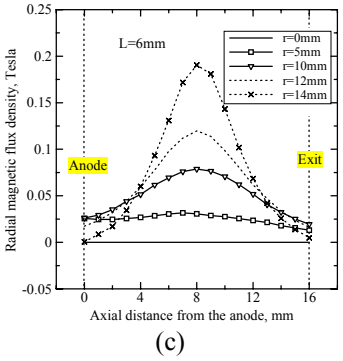

(c)

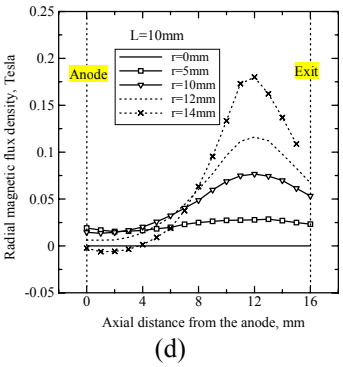

(d)

Figure 4. Axial profiles of radial magnetic flux density of TCHT-3. (a)TCHT-3A, (b)TCHT-3B(L=2mm), (c)TCHT-3B(L=6mm), (d)TCHT-3B(L=10mm).

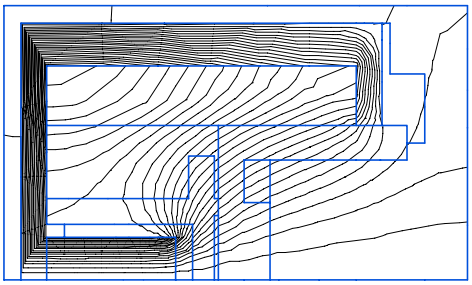

(a)

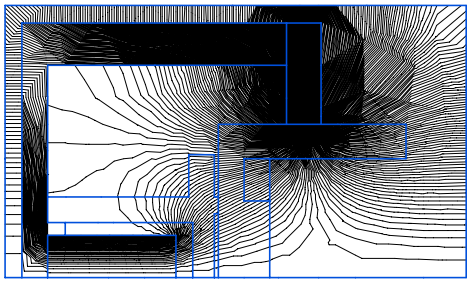

(b)

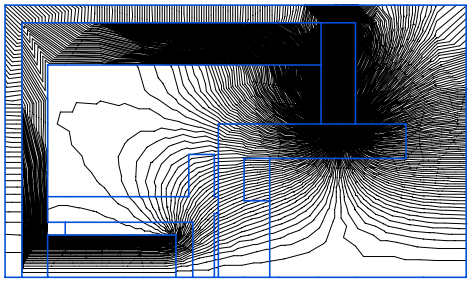

(c)

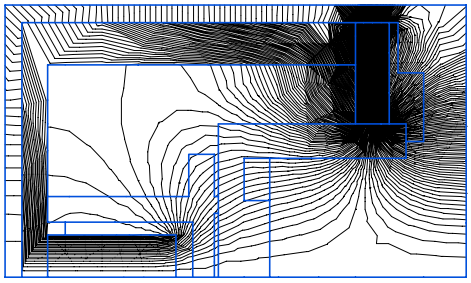

(d)

Figure 5. Magnetic field lines of TCHT-3. (a)TCHT-3A, (b)TCHT-3B(L=2mm), (c)TCHT-3B(L=6mm), (d)TCHT-3B(L=10mm).

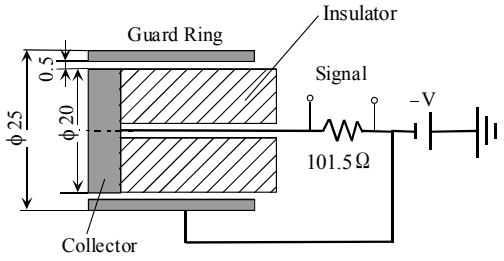

Figure 6. Cross-sectional view of Faraday probe.

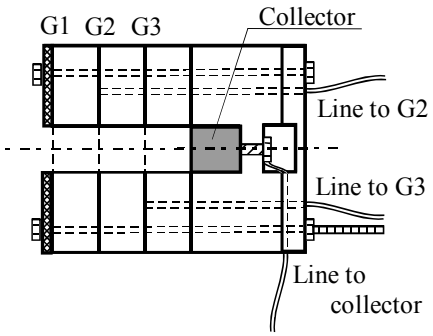

Figure 7. Schematic drawing of RPA.

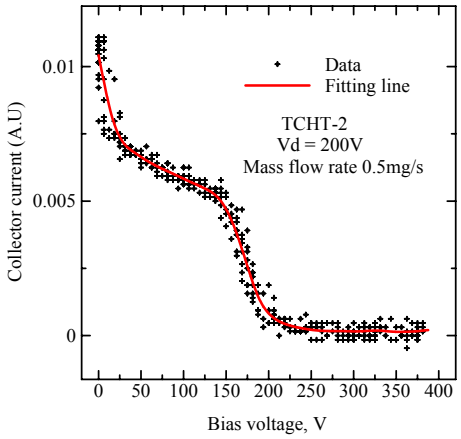

Figure 8. Typical trace of RPA.

direction is radial direction. By changing the outer iron cylinder , we varied the distance L defined as the distance from the anode to the edge of ring-like magnet to examine the effect of magnetic field profile on the thrust performance. The distance L is set to 2, 6 and 10mm. To distinguish TCHT-3B by the distance L, we call them TCHT-3B(L=2mm), TCHT-3B(L=6mm) and TCHT-3B(L=10mm), respectively. The wall materials of the discharge chambers of TCHT-2 and TCHT-3 were Boron Nitride (BN). Notice that outer coil was not used under operation of TCHT-3B. Therefore, TCHT-3B has advantage to save input power for magnetic coil.

Figure 3(a) shows the calculated axial profiles of radial magnetic flux density of TCHT-2. The ratio of inner to outer magnetic coil currents is set to 1:1, and each current is set to 2A. The condition of coil currents was used in all experiments below this sections. Figure 3(b) shows the calculated magnetic field lines. It has large axial component of magnetic flux density and forms magnetic nozzle, which never exists in SPT. Hence, the mechanism that suppresses electron motion to the anode of TCHT-2 may differ from that of SPT. For example, magnetic mirror effect may suppress electron motion to the anode.

Figures 4 and 5 show the calculated magnetic field of TCHT-3A and TCHT-3B(L=2, 6, 10mm), respectively. We can see that TCHT-3A has similar magnetic field configuration to TCHT-2. In the case of TCHT-3B, the peak of radial magnetic flux density gets toward the thruster exit, as the distance L increases.

The vacuum facility mainly consists of a water-cooled stainless steel vacuum tank 1.2 m in diameter x 2.25 m long, two compound turbo molecular pumps, several DC power supplies and a thrust measurement system[9,10]. The vacuum tank pressure is kept in the range of 2×10^{-2} Pa under operations. By using the oil-free turbo molecular pump system, clean and high vacuum environment is produced.

Thrusts are measured by a pendulum method. A Hall thruster is mounted on a thrust stand suspended with an aluminum bar, and the position of the thrust stand is detected by an eddy-current-type gap sensor (non-contacting micro-displacement meter).

The hollow cathode (Iontech HCN-252) is employed as the electron emission source. Propellant gas is injected into the discharge chamber through four lines behind the anode. Xenon is used as the propellant and working gas of the cathode.

B. Faraday probe

A Faraday probe shown in Fig. 6 is employed for ion current measurement. The Faraday probe consists of a collector disk with a diameter of 20mm and a guard ring with an outer diameter of 25mm. The guard ring that is biased at the same voltage shields the collector from low energy ions arriving from non-axial directions and also reduces electrostatic edge effects[11,12]. The spacing between the collector and the guard ring is 0.5mm. The probe is placed at 27.5cm downstream from the exit plane of TCHT-2, and it is swept $\pm$ 90° from the thruster center line through the plume in 15° increments. The collector and the guard ring were

biased at –27V. The current drawn by the Faraday probe was determined by measuring the voltage across a current shunt.

C. Retarding potential analyzer (RPA)

A retarding potential analyzer (RPA) is employed for ion energy measurement. It is composed of a current collector which is shielded by biased grids. Figure 7 shows the RPA with three grids(G1, G2, G3). The first grid G1 is floated to reduce plasma perturbation; the second one G2 is biased at –27V to repel electrons, and the third grid G3 potential is varied to repel selected ions. The diameter of the inlet is 10mm; the distance between each grid is 10mm, and the distance between the third grid and the collector is 10mm. The RPA is placed on the thruster axis at 35cm downstream from the exit plane of TCHT-2. Figure 8 shows typical V-I characteristics of RPA with a mass flow rate of 0.5mg/s at a discharge voltage of 200V. Sharp decrease in collector current was observed at 0-50V and 150-200V.

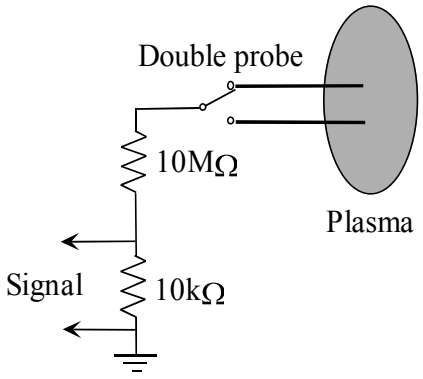

Figure 9. Electrical setup for floating potential measurement.

D. Electrostatic double probe

The strong magnetic field in the Hall thruster complicates probe diagnostics. Single probe technique is significantly affected by magnetic field. Besides, Hall thruster plasma is quite sensitive to probe immersion[13]. From these considerations, the double probe technique was chosen for the diagnostics of the Hall thruster plasma. Since the double probe is operated near the floating potential, it is not significantly affected by the magnetic field. And because the double probe does not draw the net current from plasma, it can suppress the perturbation of Hall thruster plasma. Using the double probe, electron temperature and electron number density were measured. And floating potential was measured to calculate plasma potential. Figure 9 shows the electric setup to measure floating potential. The one electrode is connected to ground through 10MΩ and 10kΩ resistance, and no bias voltage was applied. The signal obtained by the 10kΩ resistance was taken as floating potential. The average value taken from two electrodes was used as the floating potential of each measurement point. Floating potential is commonly determined by applying bias voltage with respect to ground to the electrode and finding the voltage that makes probe current zero. Since probe current is small but not zero using the method shown in Fig. 9 , the floating potential seems to be less accurate than that with common method. However, the common method disturbed the thruster operation, and very little difference between two methods was observed by test at the downstream region(about 8cm downstream from thruster exit). Therefore, we employed the simple method without bias voltage.

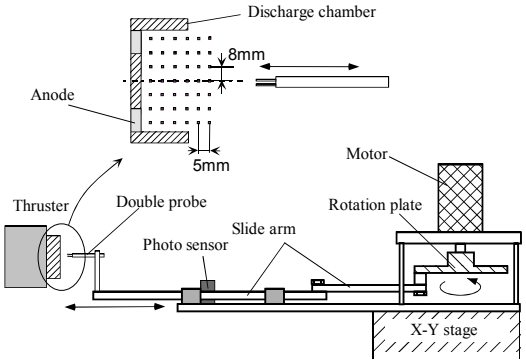

Figure 10. Double probe measurement system.

The double probe consists of a 0.4mm diameter, 5.5mm long tungsten electrodes supported by a double-bore ceramic tube. The probe is mounted on probe-inserting device on the X-Y positioning system. The probe-inserting device consists of a motor, a rotating disk and slide arm, and it allows the probe to be inserted into, and removed from, the thruster on a time scale under 2 sec. The probe setup is shown in Fig.10. Measurements along the thruster axis(r = 0mm), r = ±8, ±16, ±24mm were performed at seven axial locations: z = -10, -5, 0, 5, 10, 15, 20mm. The axial position z indicates the distance from the thruster exit towards the anode.

III. Results and Discussion

A. Thrust performance of TCHT-2

Table 1 shows the thrust performance of TCHT-2 with mass flow rates of 0.5mg/s and 1.0mg/s at a discharge voltage of 200V. The detail performance characteristics of TCHT-2 are presented in Ref. 9. The specific impulse and thrust

Table 1. Thrust performance of TCHT-2.

	Id	Isp	η_T	Power
0.5mg/s	0.65A	1200sec	27%	130W
1.0mg/s	1.54A	1450sec	31%	308W

efficiency with 1.0mg/s are higher than those with 0.5mg/s.

B. Ion current distribution

Figure 11 shows the ion current distribution for a mass flow rate of 1.0mg/s at a discharge voltage of 200V. TCHT-2 has a broad ion current distribution compared with SPT[14,15]. The plume divergent half angles for 0.5mg/s and 1.0mg/s, which are based on 95% of the total ion beam current, was 79 and 78 degrees, respectively. Since TCHT-2 has relatively large axial magnetic field, it is expected that radial electric field forms. Hence, ions are accelerated in not only axial direction but also radial direction, and plume divergence increased. The calculated propellant utilization for 0.5mg/s and 1.0mg/s was 0.97 and 1.3, respectively. Now, we consider backpressure effect on the propellant utilization. The back pressure of 1.4×10^{-4} Torr (1.86×10^{-2}Pa) with 1.0mg/s is slightly higher than that of 1.2×10^{-4} Torr(1.6×10^{-2}Pa) with 0.5mg/s. When backpressure increases, slow ions are generated by charge exchange (CEX) collisions. Then, these slow CEX ions are drawn toward the probe, and these ions increase the ion current density at large angle; that is, CEX ions can increase plume divergent angle and affect total ion current. However, the divergent angle for each mass flow rate was almost equal. Hence, the difference of propellant utilization is not owing to the difference of backpressure. Therefore, propellant utilization for 1.0mg/s was qualitatively higher than that for 0.5mg/s.

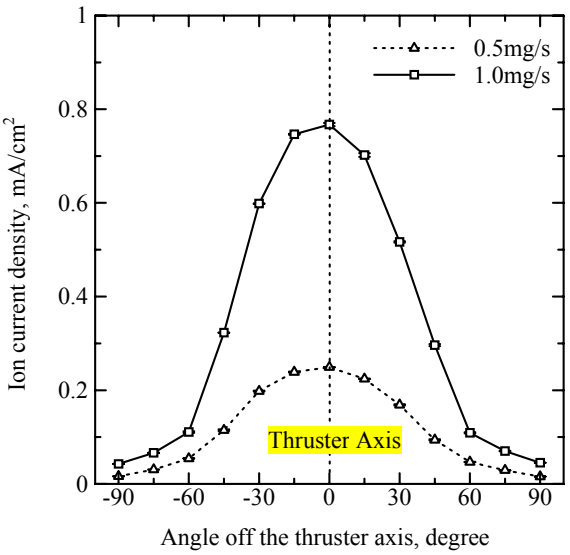

Figure 11. Ion current density distribution of TCHT-2 for two mass flow rates.

C. Ion energy distribution

Figure 12 shows the ion energy distribution for mass flow rates of 0.5mg/s and 1.0mg/s. In all conditions, low energy(<50eV) peaks are discernable. These peaks may be due to the low energy CEX ions. Hence, the peak is not related to acceleration by the thruster directly. The higher peaks are sensitive to the discharge voltages. Therefore, the peaks are due to accelerated ions by the thruster. We can see that the peak energy with 1.0mg/s is higher than that with 0.5mg/s. For instance, the peak energy with 0.5mg/s and 1.0mg/s at 200V are 172eV and 187eV, respectively. Since the neutral number density with 0.5mg/s is smaller than that with 1.0mg/s, the mean free path is longer. As a result, neutrals tend to reach more downstream region without ionization. Since the plasma potential drops at the downstream region, ions generated in the region gain lower ion energy. And it results in lower peak energy.

From the results of the ion current distribution and ion energy distribution, the decline in thrust performance with low mass flow rate is attributed to decrease of neutral number density in the discharge chamber. Hence, it is necessary to downsize the radius of discharge chamber for low power Hall thruster.

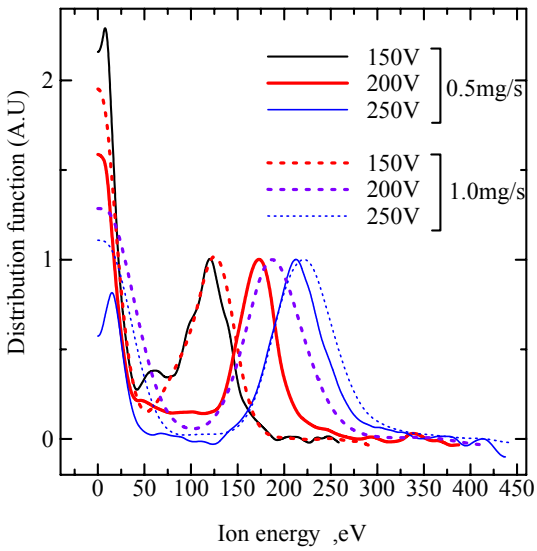

Figure 12. Ion energy distribution of TCHT-2.

D. Plasma characteristics of TCHT-2

Figure 13 shows the electron temperature, electron density and plasma potential distributions at a mass flow rate of 0.5mg/s and at a discharge voltage of 200V. Electron number density increases at the

upstream region on the thruster axis. This region is near the 'throat' of magnetic nozzle. The electron temperature ranges from 8 to 20eV. The electron temperature increases near the anode and throat of magnetic nozzle. Thus, electron fluid is compressed by the magnetic nozzle. From the measured floating potential V_f, we calculated plasma potential V_p using the following simple equation;

$$V_p = V_f + T_e \ln\left[0.654\left(\frac{m_i}{m_e}\right)^{1/2}\right] \cong V_f + 5.75T_e \quad (1)$$

where T_e, m_i and m_e are electron temperature, ion mass and electron mass, respectively. Though this method of finding plasma potential is less accurate than the more common emissive probe method, we can obtain plasma potential qualitatively. Plasma potential near the anode is slightly higher than discharge voltage because of high electron temperature. Plasma potential drops sharply from the anode. From the electron temperature and plasma potential distributions, it is expected that ionization/acceleration region is located near the anode in which strong radial magnetic field exists.

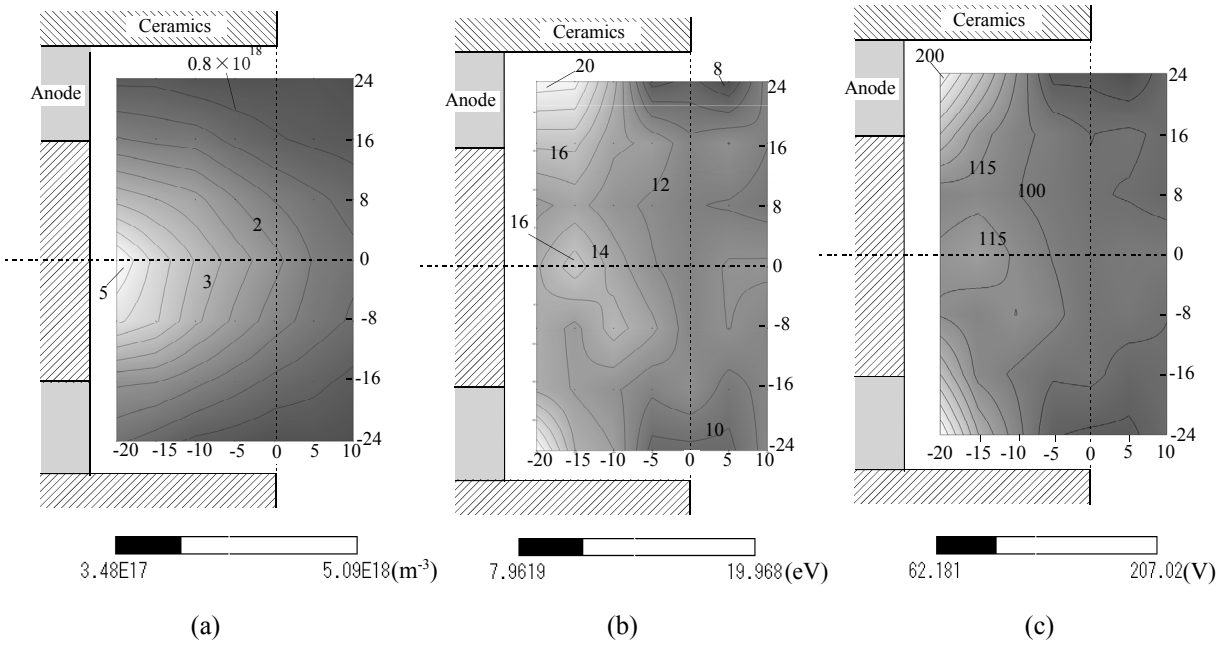

Figure 13. Plasma properties in the discharge chamber of TCHT-2 at a mass flow rate of 0.5mg/s. (a)Electron number density, (b)Electron temperature, (c)Calculated plasma potential.

E. Miniaturization of Hall thruster with circular cross-sectional discharge chamber

We designed downsized Hall thruster, named TCHT-3A and TCHT-3B. Although TCHT-3A has a permanent magnet on the thruster axis, TCHT-3A is simply miniature thruster of TCHT-2. Table 2 shows the thrust performance of TCHT-3A for two mass flow rates of 0.37mg/s and 0.5mg/s. The thrust performance for 0.5mg/s is lower than that for 0.37mg/s. Becasuse the discharge current is propotional to mass flow rate, the propellant utilization will be equal. The volume-to-surface ratio of TCHT-3 is 4.87(mm), and that of TCHT-2 is 8.97(mm). Hence, wall loss increased, and thrust performance declined in the case of 0.5mg/s with TCHT-3A. Accordingly, we employed new magnetic circuit for TCHT-3B. The special features of

Table 2. Thrust performance of TCHT-3A

	Id	Isp	η_T	Power
0.37mg/s	0.74A	1420sec	24%	148W
0.50mg/s	1.0A	1310sec	20%	200W

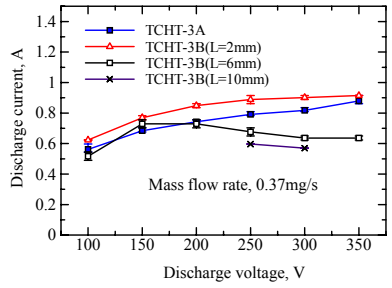

(a)

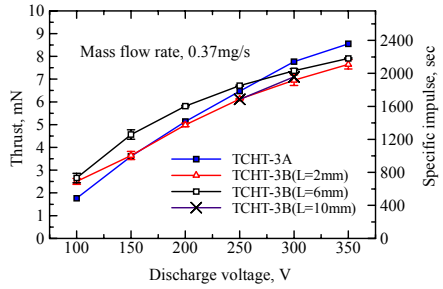

(b)

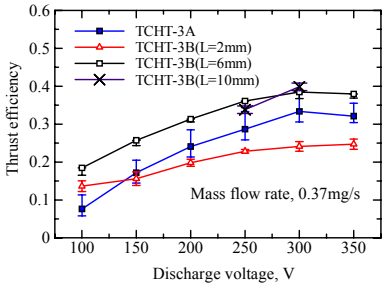

(c)

Figure 14. Thrust performance versus discharge voltage, (a)discharge current, (b)thrust and specific impulse, (c)thrust efficiency,

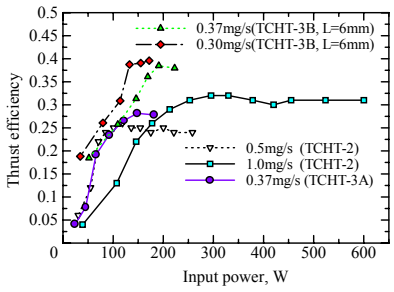

Figure 15. Variation of thrust efficiency relative to input power.

TCHT-3B is that it has a ring-like permanent magnet instead of outer coil. And TCHT-3B has the peak of radial magnetic flux density at more downstream region than TCHT-3A has. As mentioned above, the ionization/acceleration region is located near the region in which the strong radial magnetic flux density exists. Therefore, applying the strongest radial magnetic field at the downstream region will suppress wall loss and electron current to the anode and enhance thrust performance because the ionization/acceleration region gets toward downstream region. In this section, we compare the thrust performance of TCHT-3A and TCHT-3B(L=2, 6, 10mm) with a mass flow rates of 0.37mg/s. The outer coil current of TCHT-3A is set to 2A.

Figure 14(a)shows discharge current-voltage characteristics. It was difficult to operate TCHT-3B(L=10mm) except for 250 and 300V. In the case of TCHT-3B(L=2mm), the discharge current is relatively large for all discharge voltages compared with TCHT-3A and TCHT-3B(L=6, 10mm). The discharge current with TCHT-3B(L=10mm) is the smallest. The discharge current with TCHT-3B(L=6mm) increases with the discharge voltage and reaches a peak at 150V. After it decreases slightly, and it kept constant. Except for 150V, the discharge current with TCHT-3B(L=8mm) is smaller that with TCHT-3A. Figure 14(b) shows thrust and specific impulse as a function of discharge voltage. The thrust and specific impulse with TCHT-3B(L=6mm) are the largest in the range of 100-250V. However, at 300 and 350V, the thrust and specific impulse with TCHT-3A are larger than those with TCHT-3B(L=6mm). The thrust and specific impulse with TCHT-3B(L=2mm) and TCHT-3B(L=10mm) are relatively small. Figure 14(c) shows thrust efficiency as a function of discharge voltage. Thrust efficiency in each case increases with discharge voltage. The highest thrust efficiency was obtained with TCHT-3B(L=6mm).

In the case of TCHT-3B(L=10mm), the ionization region is located at most downstream region. At the downstream region, the neutral number density decreases compared to the upstream region because of diffusion. As a result, the propellant utilization decreased, and the discharge current and specific impulse decreased. In the case of TCHT-3B(L=6mm), the ionization region shifted more upstream. However, it is not located near the anode like TCHT-3A. Hence, the propellant utilization was enhanced compared to TCHT-3B(L=10mm). And ion loss and electron current to the anode were suppressed compared to TCHT-3A. Therefore, the discharge current with TCHT-3B(L=6mm) was smaller than that with TCHT-3A, and specific impulse was higher than that with TCHT-3A. The higher specific impulse with TCHT-3A at 300 and 350V may be attributed to multiply charged ions, considering increase in discharge current. In the case of TCHT-3B(L=2mm), the ionization region is located at most upstream region. Hence, ion loss and electron current to the anode increased. As a result, the discharge current increased and specific impulse decreased. However, the mechanism is unclear that discharge current with TCHT-3B(L=2mm) was larger than that with TCHT-3A, considering the peak of radial magnetic flux density with TCHT-3B(L=2mm) was located more downstream than that with TCHT-3A.

These results indicated that the optimal distance L that maximize thrust performance exists. Figure 15 shows the thrust efficiency versus input power. TCHT-3B(L=6mm) with 0.30mg/s successfully achieved high thrust efficiency of 26-39% in the input power range of 80-170W.

IV. Conclusion

We carried out plasma measurements of Hall thruster with circular cross-sectional discharge chamber, named TCHT-2, and examined downsized Hall thrusters named TCHT-3A and TCHT-3B. Ion current density measurement of TCHT-2 by means of Faraday probe showed that the plume divergent angle was about 80 degrees regardless of mass flow rate and that the propellant utilization for 1.0mg/s was higher than that for 0.5mg/s. Ion energy measurement using RPA indicated that the efficiency of acceleration for 1.0mg/s was higher than that for 0.5mg/s. From the electron temperature and plasma potential inside discharge chamber obtained by double probe, the ionization/acceleration region is located at which strongest radial magnetic field exists. TCHT-3B indicated that by adjusting the position of peak of radial magnetic flux density, the thrust performance was enhanced.

References

[1] Khayms,V., and Martinez-Sanchez,M., " Fifty Watt Hall Thruster for Microsatellites," Micropropulsion for Small Spacecraft, Progress in Astronautics and Aeronautics , 187(2000),Chap. 9, Edited by M. M. Micci and A. D. Ketsdever.

[2] Jacobson, D., and Jankovsky, R., " Test Results of a 200W class Hall Effect Thruster," 34th Joint Propulsion Conf., AIAA Paper 98-3791 ,1998.

[3] Hruby, V., Monheiser, J., Pote, B., C. Freeman and W. Connolly., "Low Power Hall Thruster Propulsion System," 26th International Electric Propulsion Conference, Kitakyushu, Japan, Paper No.IEPC-99-092.

[4] Zhurin, V., V., Kaufman, H., R., and Robinson, R., S., " Physics of Closed Drift Thrusters," Plasma Sources Science and Technology, 8(1999), R1-R20.

[5] Raitses, Y., and Fisch, N., J., "Parametric Investigations of a Nonconventional Hall Thruster," Physics of Plasmas,8(2001), pp.2579-2586.

[6] Smirnov, A., Raitses, Y., and Fisch, N., J., "Parametric Investigation of Miniaturized Cylindrical and Annular Hall Thrusters, Journal of Applied Physics," 92(2002), pp.5673-5679.

[7] Smirnov, A., Raitses, Y., and Fisch, N., J., " Plasma Measurements in a 100W Cylindrical Hall thruster," Journal of Applied Physics, 95(2004), pp.2283-2292.

[8] Smirnov, A., Raitses, Y., and Fisch, N., J., "Electron Cross-field Transport in a Low Power Cylindrical Hall Thruster," Journal of Applied Physics, 95(2004), pp.2283-2292.

[9] Shirasaki, A., Tahara, H., and Yoshikawa, T., "Performance Characteristics of Low Power Hall Thrusters with Circular Cross-sectional Discharge Chambers," Proceedings of the 24th International Symposium on Space Technology and Science, ISTS 2004-b-35, pp. 203-208, 2004.

[10] Shirasaki, A., Tahara, H., and Yoshikawa, T.,"Operational Characteristics of Cylindrical Hall Thrusters," 28th International Electric Propulsion Conference, Toulouse, France, Paper No. IEPC-03-051, 2003.

[11] Walker M., L., R., Victor A., L., Hofer R., R., and Gallimore, A., D., "Effect of Backpressure on Ion Current Density Measurements in Hall Thruster Plumes," Journal of Propulsion and Power, Vol. 21, No. 3, 2005, pp. 408-415.

[12] Rovey, J., L., Walker, M., L., R., and Gallimore A., D., "Evaluation of a Magnetically-Filtered Faraday Probe for measuring the ion current density profile of a Hall Thruster", 40th AIAA/ASME/ASEE Joint Propulsion Conference and Exhibit 11-14, Florida, 2004,AIAA paper 2004-3948.

[13] Haas, J., M., and Gallimore, A., D., "Internal Plasma Potential Profiles in a Laboratory-model Hall Thruster," Physics of Plasmas, Vol.8, No.2, 2001, pp.652-660.

[14] Belikov, M., B., Gorshkov O., A., and Rizakhanov, R., N.,"The Output Parameters and Angular Plume Characteristics of Low-power Hall Thrusters," 26th International Electric Propulsion Conference, Kitakyushu, Japan, Paper No.IEPC-99-094, 1999.

[15] Kozubsky, K., Kudriavtzev, S., Pridannikov, S.,"Plume Study of Multimode Thruster SPT-140, 26th International Electric Propulsion Conference, Kitakyushu, Japan, Paper No.IEPC-99-073, 1999.